

Applying a through-casing acoustic imaging technique to identify gas migration paths in a salt body

Tom Bradley,^{1*} Douglas Patterson¹ and Xiao-Ming Tang² introduce a method developed to image geological structures in a cased borehole by using dipole array acoustic waveform data. The resulting fracture connectivity model can reveal migration pathways for the gas within a salt body.

A moderately deviated well was drilled through a thick evaporite sequence in the North Sea. The evaporite body was assumed to be homogeneous; however, during drilling gas shows were observed by the mudloggers in the halite section. No openhole wireline logs or logging while drilling was acquired over the interval of interest. After casing had been set a wireline gamma ray and full-wave monopole and dipole acoustic log were acquired over the interval of interest.

It was questioned if the origin and migration paths of the gas could be determined by using the available data. It was proposed that a newly developed near-wellbore acoustic imaging technique could be applied to through-casing dipole acoustic data in an attempt to identify and characterize possible gas migration paths in the evaporite sequence. It is believed that this type of near-wellbore imaging has never previously been applied in a cased-hole borehole.

The results indicated that the acoustic imaging processing detected geologic reflector structures through the casing up to 70 ft (21.3 m) away from the borehole. Two types of reflectors with different dip angles were mapped out by the imaging. The low dip-angle reflectors are assigned to the formation beds/structures crossing the borehole. High-angle reflectors correspond to fractures and/or faults of large extent in the formation. These acoustic imaging results were then compared to the gas observed during drilling and showed a direct correlation to the high-angle reflectors. This technique made it possible to estimate the fracture presence away from the borehole and pathways for gas migration into the borehole.

Theory of near-wellbore imaging

The goal of acoustic reflection imaging processing of Cross Multipole Array Acoustilog F1 (XMAC-F1) dipole waveform data is to map the geologic structure away from

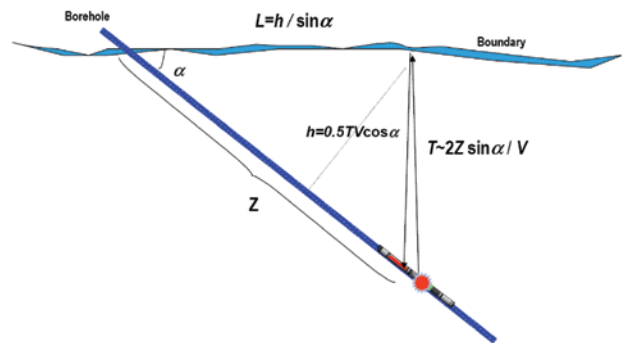


Figure 1 Schematic of an angled reflector cutting a borehole.

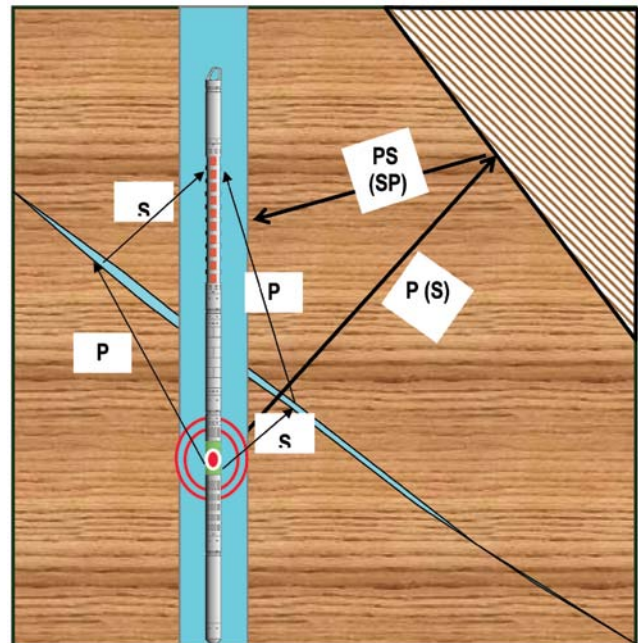


Figure 2 Illustration of mode conversion of acoustic waves at boundaries in the formation. As the energy crosses or reflects at a boundary it can undergo a mode conversion from P to S and vice versa. In an acoustic reflection image, these mode conversions appear as noise and/or spurious reflectors.

¹ Baker Hughes.

² China University of Petroleum, Qingdao, China.

*Corresponding author, E-mail: tom.bradley@bakerhughes.com

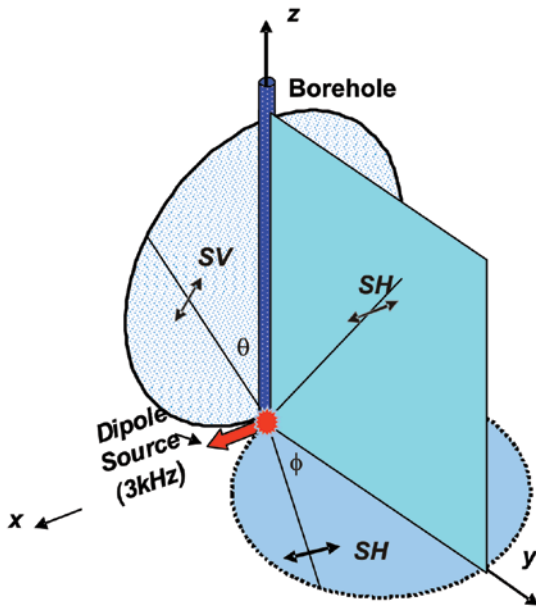


Figure 3 Dipole radiation pattern in a borehole from a single dipole source. The dipole source is aligned in the X direction. The radiated SH and SV components propagate in all directions respectively so enabling reflectors of any orientation to be imaged (Tang and Patterson, 2009).

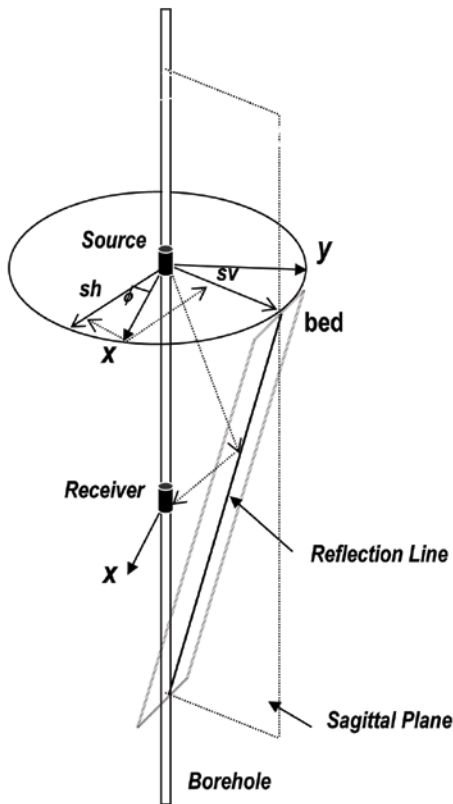


Figure 4 Schematic of imaging of reflector planes that are not aligned with the dipole source direction. The formation shear wave generated by the dipole source can be decomposed into an SV wave that points to the reflector as described in Eqs. 3 and 4a, and an SH wave that polarizes parallel to the reflector as described in Eq. 4b.

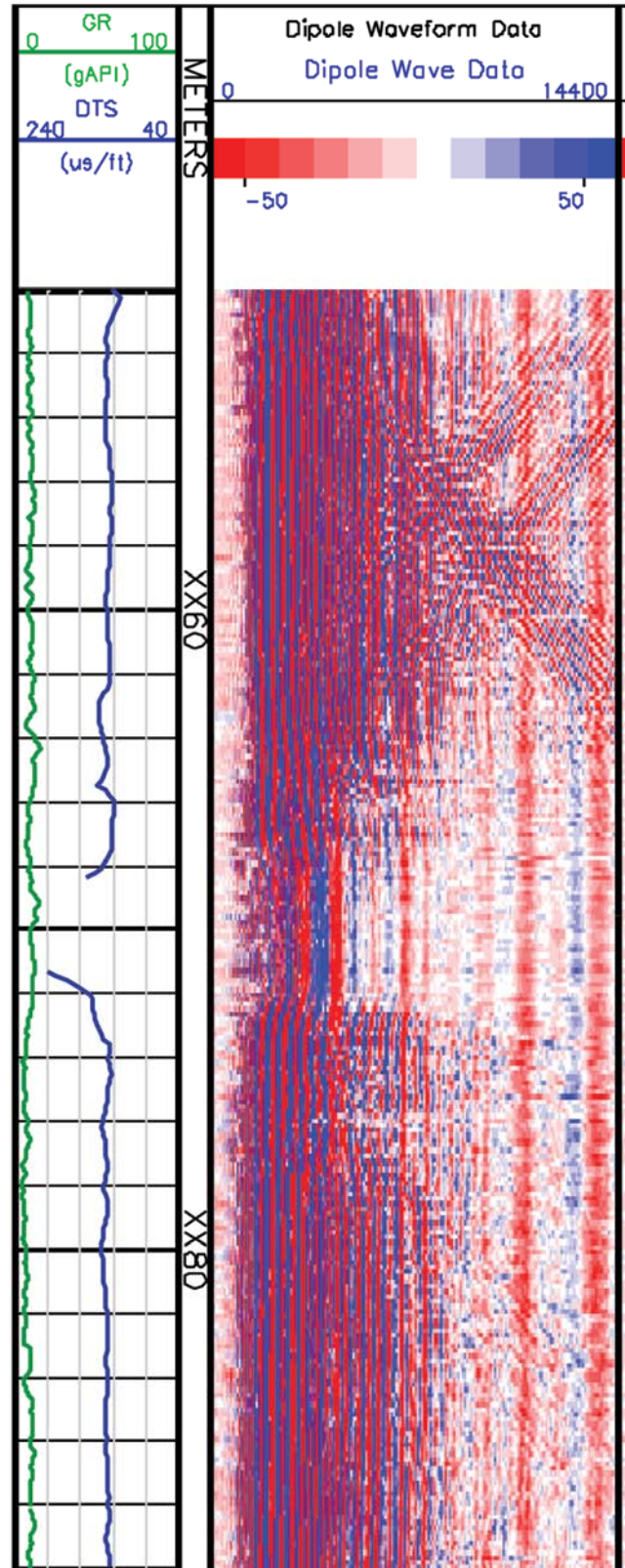


Figure 5 Example of dipole waveform showing chevron pattern reflection artefacts. These can be attributed to reflections from planar features in the formation near to the wellbore.

the borehole. When the acoustic property of the structure is significantly different from the ambient formation, the structure reflects acoustic energy generated by the acoustic logging tool back to the borehole. Processing the reflected acoustic waves allows the structure to be imaged.

The borehole acoustic reflection technique was originated by Hornby (1989). When full-wave acoustic data is recorded it contains both the direct formation arrivals (compressional, shear, and Stoneley) and also reflection events from the acoustic energy being reflected off formation features and back to the receivers.

In conventional acoustic slowness analysis, the reflection events are considered to be noise and measures are taken to minimize these, however, in the near-wellbore reflection imaging technique these reflections are in fact the signal of interest and the direct arrivals are the noise signal. Sophisticated filtering techniques need to be applied to suppress the direct formation arrivals. A combination of a finite impulse response frequency bandpass filter and Pseudo-FK depth based filter are applied. The purpose of the finite impulse response (FIR) filter is to isolate the frequencies of interest and the Pseudo-FK filter to minimize the direct formation arrivals which are often two orders of magnitude larger than the reflected waves.

This results in a wave trace that will contain mainly the reflection events. These reflection events are from when the tool is below and above the reflecting plane. Before the reflector can be migrated it is necessary to separate these into individual up-going and down-going reflection wave traces. A parametric wave separation technique (Tang et al., 2007) is then applied to separate the up-going and down-going reflections representing up-dip and down-dip structures in the ambient formation. These can then be migrated from an event in the time domain to an image in the radial distance domain using well established seismic techniques and the conventional slowness data computed from the near wellbore region.

How far can we see?

The distance from the borehole that reflectors can be imaged is controlled by several key factors:

- Length of the recorded wave train
- Formation slowness
- Angle of the reflector to the borehole
- Formation attenuation

Figure 1 shows the schematic of a reflector cutting the borehole.

For a reflector to be imaged, the time taken for the wave to travel from the transmitter to the reflector to the receiver has to be less than the recording time of the tool, and the return signal has to be above the tool receiver's noise threshold. This travel time is directly related to the

formation velocity and the angle of the reflector relative to the tool. When the distance to the reflector is large relative to the transmitter-receiver spacing of the tool the geometric parameters given in Figure 1 can be related by Eq. 1.

$$h \approx 0.5TV \cos \alpha, \tag{Eq. 1}$$

where h is the perpendicular distance from the borehole to the reflecting point on the plane, T is the two-way travel time of the reflecting waveform, V is the velocity of the formation, and α is the angle between the plane and the borehole.

It can be seen from Eq. 1 that there are two special cases. When the reflector is parallel to the borehole and the distance is greater than the receiver-transmitter spacing, as $\cos \alpha$ approaches one the distance imaged approximates to 0.5TV. If the reflector is perpendicular to the borehole as α approaches 90°, $\cos \alpha$ approaches zero so the reflector will not be imaged. Experience shows that it is generally

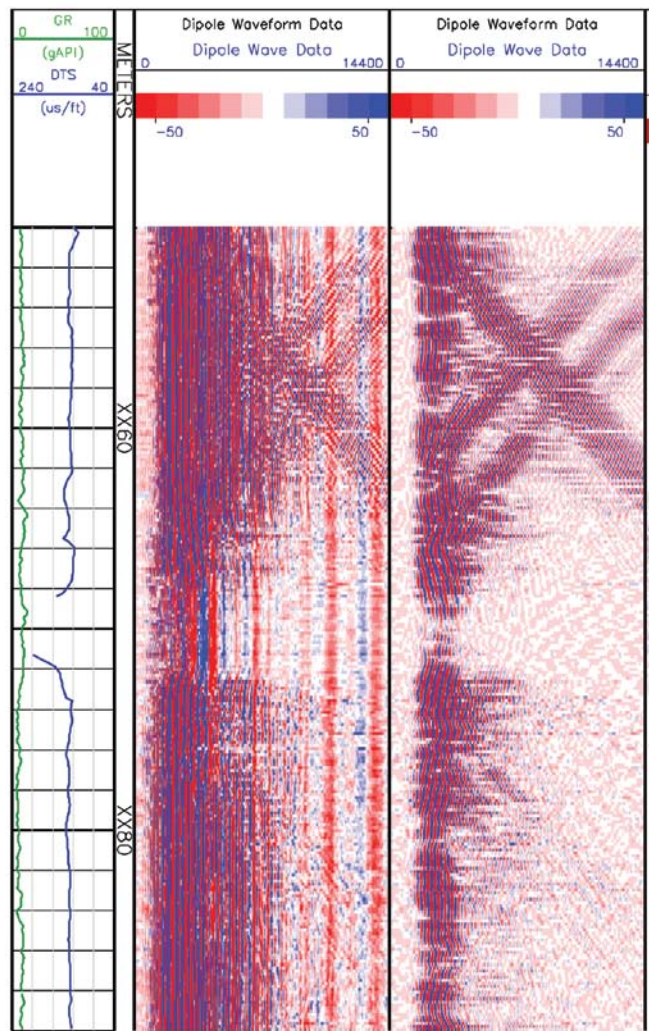


Figure 6 Dipole wave data before (left) and after (right) application of a Pseudo-FK filter. Note how direct formation wave arrivals have been minimized.

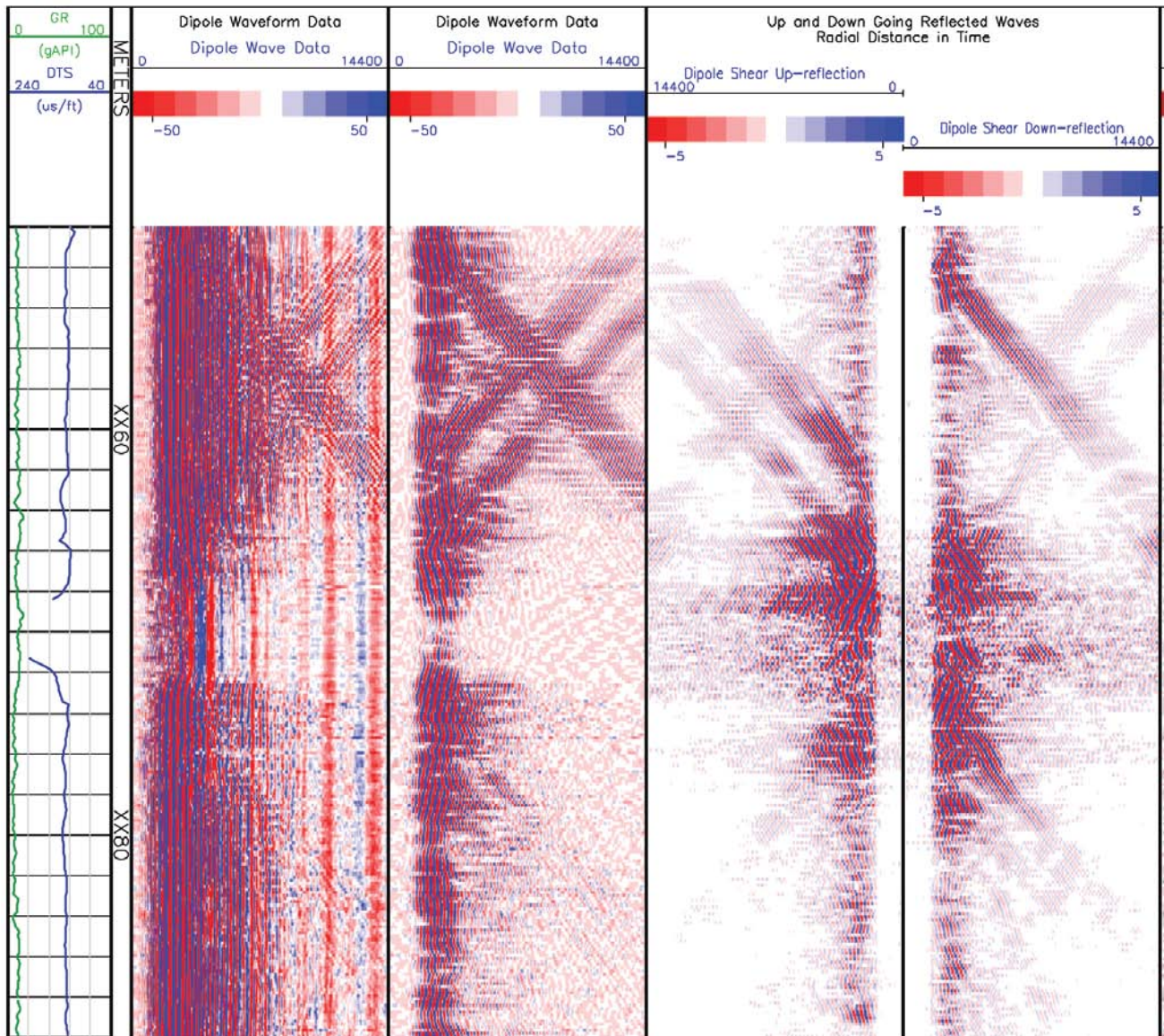


Figure 7 Waveform data after wave-separation processing is applied. Note how up-going (left) and down-going (right) reflections are now isolated.

possible to image reflectors with an intersection angle with the borehole greater than 20° .

Near-wellbore imaging using dipole waveform data

The traditional reflection imaging technique using monopole data does suffer from some shortcomings. The radiation pattern of the P and SV waves generated by a monopole source are highly influenced by the presence of the borehole (Meredith, 1990). Therefore in certain directions wave energy will be reduced leading to any planes in these orientations being poorly imaged.

Acoustic imaging can be further complicated by mode conversions in the formation at feature boundaries. As in

Figure 2, reflection from a bed converts P (S) to PS (SP) waves, while transmission across a boundary converts P(S) to S(P) waves. This mode conversion does not satisfy the theory of reflection imaging and will appear in the image result as increased noise or spurious reflectors. The converted mode effects will be more severe for monopole-wave imaging than for dipole-shear wave imaging because the monopole energy contains components due to compressional, shear, and Stoneley waves.

Reflectors can only be imaged when the reflected wave energy is above the noise threshold of the tool. Waveform attenuation is influenced by two factors; the geometric spreading from a point source and attenuation along the waveform path. The attenuation is related to the quality

factor Q of the formation, which, denoted by AQ , can be quantified using Eq. 2.

$$AQ = e^{-\pi fT/Q} \quad (\text{Eq. 2})$$

where T is the reflection traveltime that equals wave-travel distance divided by the wave velocity and f is the frequency of the wave.

From Eq. 2, it can be seen that as the frequency of the waves used increases, attenuation of the signal amplitude also increases exponentially, reducing the radial distance that can be imaged. Monopole waves are generally high frequency and attenuate rapidly limiting the distance that can be imaged.

Using dipole shear waves for reflection imaging alleviates the disadvantages of imaging using monopole data. Compared with conventional compressional wave imaging using monopole waves around 10 kHz, an advantage of the shear wave imaging is its deeper depth of penetration and lower signal attenuation due to the low-frequency nature of the dipole waves (2 to 3 kHz). Dipole data generally contains exclusively shear energy so mode conversion and interference is much reduced.

Regarding acoustic imaging using dipole source, there is a common misconception that because dipole sources in logging tools are a directional source, then the dipole energy will propagate only in certain directions and therefore any reflectors not in these directions will not be imaged. Work done by Tang and Patterson (2009) shows that the dipole waves can radiate two types of shear waves in the formation. They are known as the SH wave polarizing in the horizontal plane, and the SV wave polarizing in the vertical plane, as illustrated in Figure 3. Therefore, there will always be a component of the dipole shear wave propagating towards a reflector of certain orientation allowing reflectors of any orientation to be imaged.

If only a single inline dipole data XX is acquired, as in the present case, the data contains both SH and SV wave reflections, as given in the following Eq. 3 (Tang and Patterson, 2009).

$$XX = SH \times \cos^2 \phi + SV \times \sin^2 \phi \quad (\text{Eq. 3})$$

Where ϕ is the angle between dipole and the reflector strike. Eq. 3 shows that it is possible to use the SH and SV wave reflections acquired by an inline dipole tool to image a formation reflector, provided the angle ϕ does not change rapidly when logging in the vicinity of the reflector (i.e., no rapid tool rotation to distort the amplitude of reflection waves in data). Neglecting formation anisotropy, the SH and SV waves travel along the same wavepath to and from the reflector with the same shear velocity. Either SH or SV waves, or both can be migrated to image the reflector.

When four-component cross dipole data is acquired both XX and YY dipole source-receiver systems will radiate and receive SH and SV waves, the four-components of the data are then combined to obtain the SH and SV reflection waves, as shown in Eqs. 4a and 4b

$$SH = xx.\cos^2 \phi + (xy + yx).\sin \phi \cos \phi + yy.\sin^2 \phi \quad (\text{Eq. 4a})$$

$$SV = xx.\sin^2 \phi - (xy + yx).\sin \phi \cos \phi + yy.\cos^2 \phi \quad (\text{Eq. 4b})$$

By minimizing the cross-components XY and YX, the strike angle of the reflector can be determined and used in the above equations to obtain the SH and SV reflection waves. Migrating the reflection data obtains an image of the reflector in the formation.

Case study: imaging gas migration paths through casing in an evaporite body

Traditionally the near-wellbore imaging technique has only been applied to openhole full-waveform data. It was believed that the technique would not work in cased holes due to factors that commonly complicate through-casing acoustic analysis, for example unknown borehole conditions behind casing, poor casing to cement bond, additional contaminant modes, and influence of casing and cement on the acoustic signal.

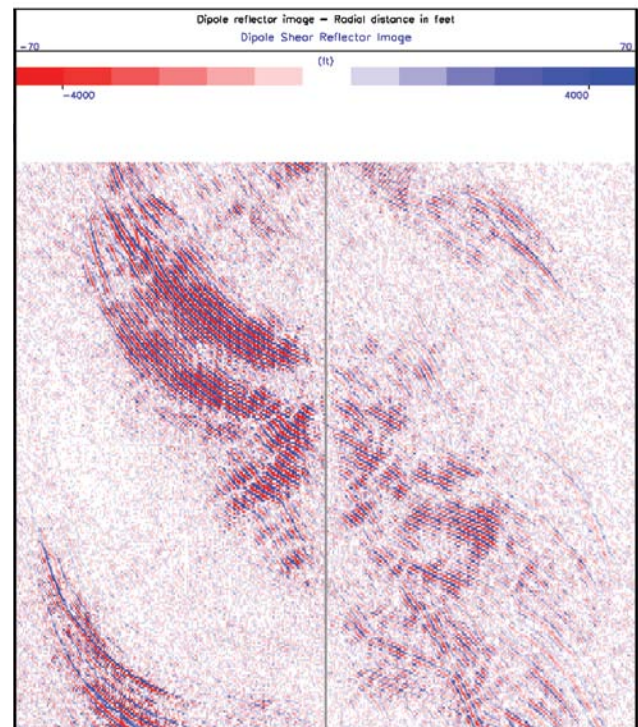


Figure 8 Data after migration to radial distance. The same 65 ft (20 m) vertical section as shown in Figs. 5-7 is displayed. The horizontal distance displayed is 140 ft (42.7 m). Reflectors with radial distance up to 70 ft (21.35 m) from the borehole axis have been imaged.

Well Technology

In the case study presented here a well was drilled through a thick halite and anhydrite evaporite sequence. Before drilling it was assumed that the sequence was relatively homogeneous and with little internal structure. However, during the drilling of this sequence multiple unexpected significant gas shows of unknown origin were observed in the mudlogging data. Casing was set before logging and then a gamma ray log and full-waveform monopole, and inline dipole acoustic data set were acquired using an XMAC-F1 acoustic tool. No other wireline log data was recorded. It was questioned if it would be possible to determine the source of the gas shows using the available data.

In this well it was observed that both monopole and dipole full-waveform data contained artefacts that could be interpreted as being caused by reflections within the formation. However, these could equally be caused by through-casing artefacts commonly seen in cased-hole full-waveform data (such as reflections at collars). It was observed that these artefacts did correspond with the gas shows. An example interval is shown in Fig. 5. The waveform data for receiver one of the tool is displayed from 0 to 14000 μ s. It was theorized that the artefacts in the dipole data were the best candidate for analysis as dipole cased-hole data is not subject to many of the artefacts often observed in monopole

data (for example, casing ring) that will be an additional source of noise as well as providing the advantages described.

Previously no near-wellbore imaging has been attempted using through-casing data, however, the agreement of these features with the gas shows suggested that the technique would be suitable for this data set.

A standard processing flow was then applied to the data. Initially a combined FIR and Pseudo-FK filter was applied to isolate the low frequency dipole slowness and minimize the direct formation arrivals to leave the reflection events. The results of this are shown in Figure 6. It can be seen that the direct formation arrivals have been minimized to leave what is thought to be the reflections from the planar features in the formation.

A waveform separation was then applied to separate the down-going and up-going waveforms to give a time-based image of the reflectors in the borehole. This image is scaled in two-way time with the borehole axis being in the centre of the image extending to 14000 μ s at the image edges, this is shown in Fig 7.

Finally the time-based dipole image is migrated to radial distance from the borehole axis using conventional seismic migration techniques and common middle point stacking (or CMP) with the wave velocity taken from the

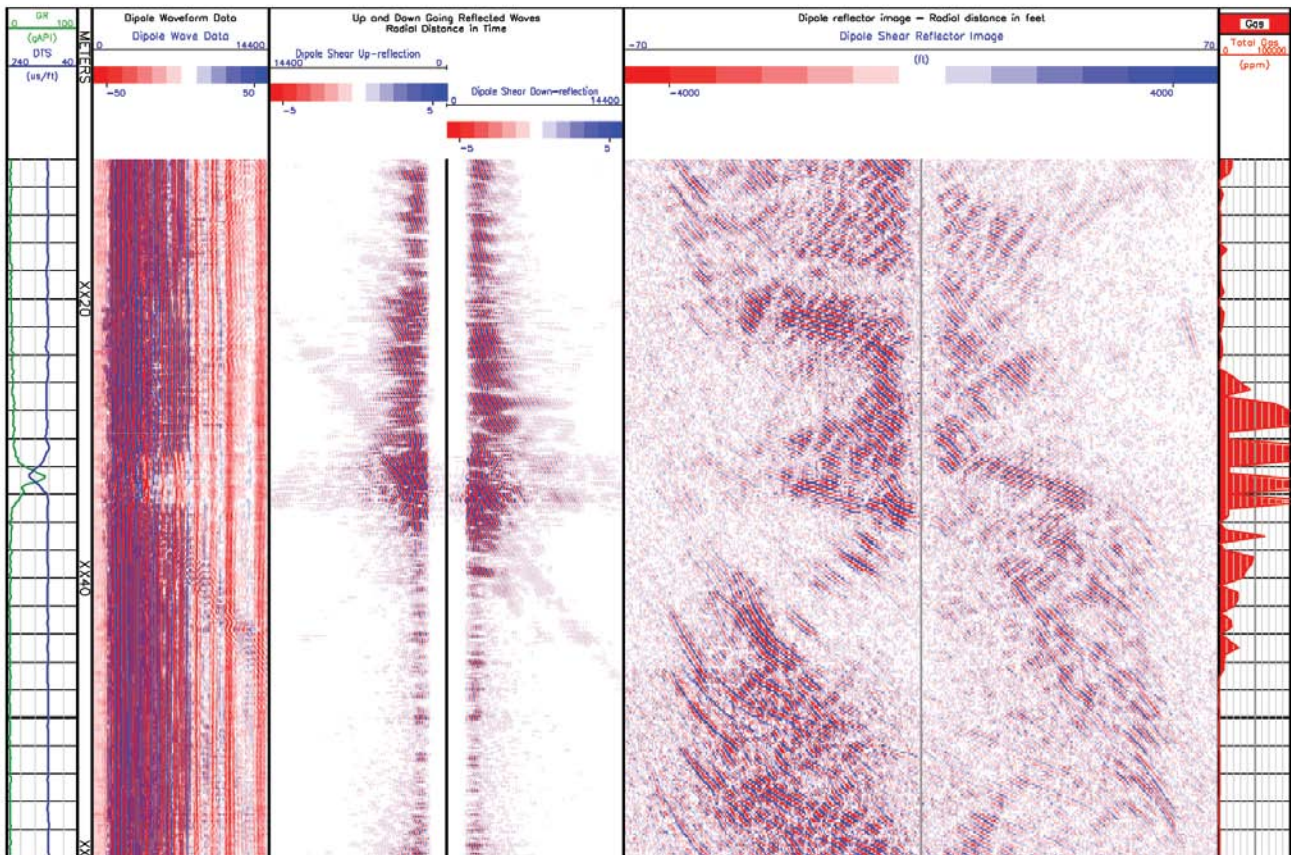


Figure 9 Near-wellbore reflector over a gas show.

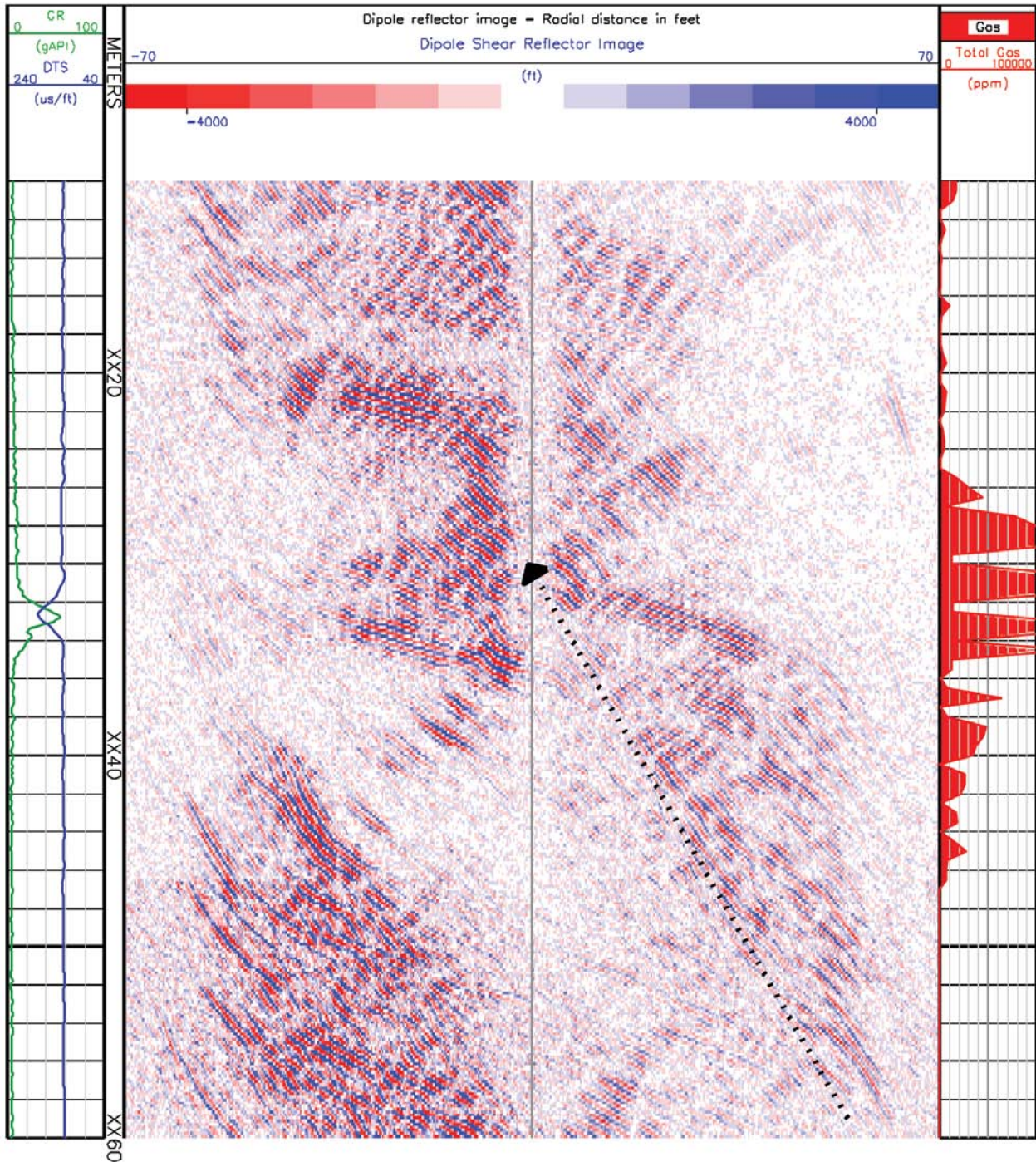


Figure 10 Example section of shear wave imaging data where the borehole penetrates a gas show. The black dashed line follows the path of a high-angle reflector that extends to the extent of the near-wellbore image. The arrowhead marks the intersection of the feature with the borehole, which corresponds with the peak gas show in the surface log data, suggesting that this feature is the migration path for the gas. Many other lower-angle features can also be observed over this interval.

conventional dipole slowness. The results of this are shown in Figure 8.

Figure 9 shows one interval where high gas shows were observed. The first track shows the gamma-ray and

shear slowness of the cased-hole interval. The second track displays the depth in metres. Track 3 displays the receiver 1 dipole waveform data. Track 4 displays the separated up and down-going reflections in time. The reflection imaging

Well Technology

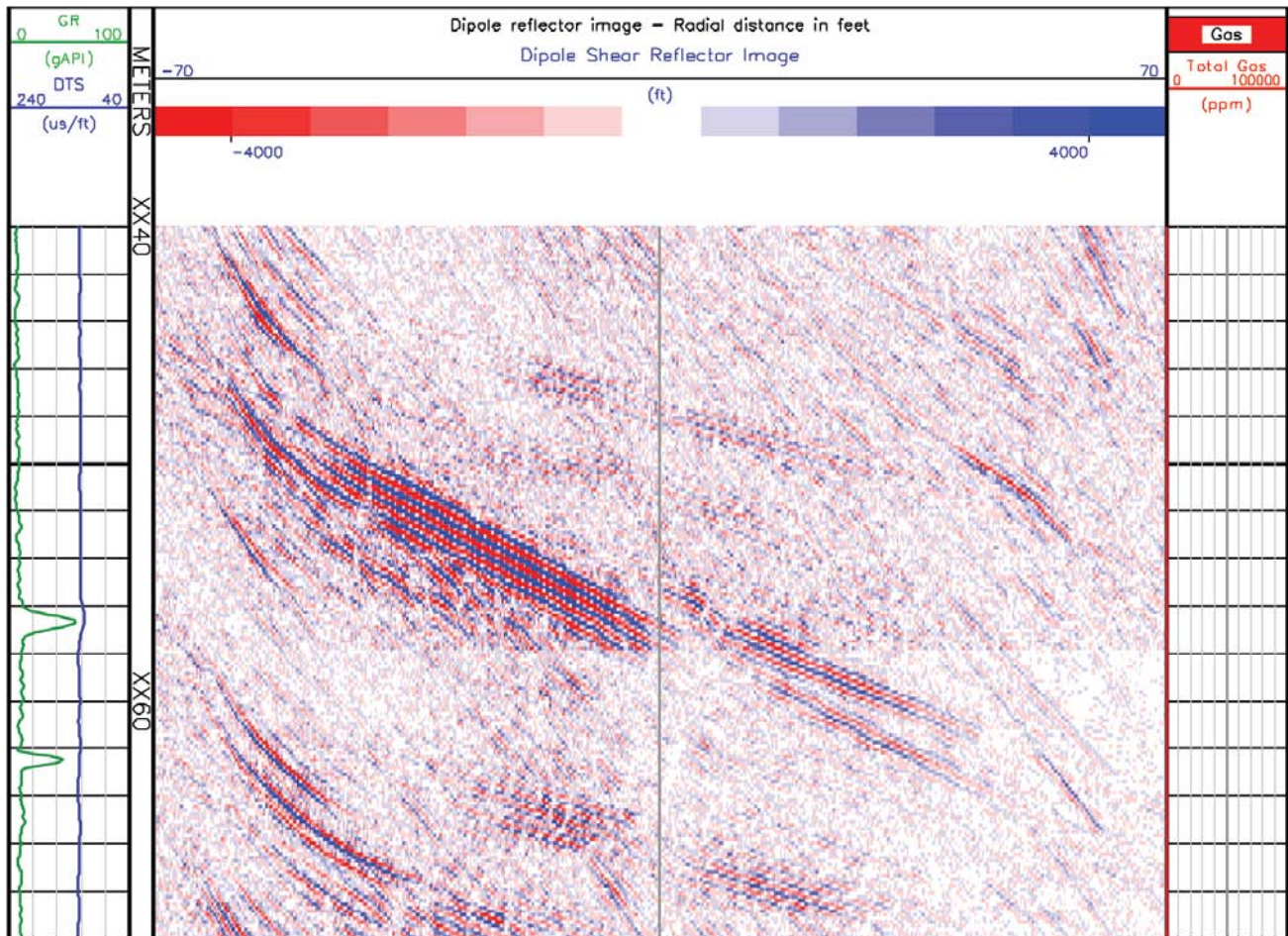


Figure 11 Example section of shear wave imaging data where a thin shale layer is present. The structure of the layer has been imaged up to 50 ft (15 m) from the borehole axis. Several other layers can also be observed.

analysis results are presented in track 5, which is discussed below. Track 6 shows the surface log total gas measurement in parts per million.

Track 5 shows the reflection imaging results in a variable density log display. The centre of the image is the borehole axis. The left and right side of the borehole are, respectively, the up-dip image migrated from the up-going reflection data and the down-dip image migrated from the down-going reflection data. The up- and down-dip images are displayed in a radial distance of 70 ft (21.35 m) from the centre of the borehole with the blue and red shading indicating the peaks and troughs of the VDL display, respectively.

An enlarged section of the migrated image is shown in Figure 10.

The near-wellbore imaging identified multiple reflector planes in the logged interval. In the interval presented in Figure 10, of particular interest was the reflector indicated by the black dashed line. This is a high-angle reflector identified in the near-wellbore image with the arrow marking the intersection of the reflector with the borehole at a depth of

XX30 m. The intersection point corresponds with the centre of the peak gas reading. This suggests that the high-angle event is a fault or fracture and is the likely migration path of the gas into the borehole.

In addition to the high-angle reflector, multiple lower-angle reflectors have been imaged which can be clearly seen in Figure 10; these are likely to be the bedding planes and other structural planes in the salt body.

Figure 11 shows an example section where a thin shalier layer (inferred from the gamma ray) is present in the salt body at XX57 m. Because of the high acoustic contrast between this and the surrounding salt a strong reflection image is obtained and it has been possible to image the structure of the layer up to approximately 50 ft (15.2 m) into the formation. Several other bedding planes parallel to the strongly imaged plane can also be observed.

Figure 12 shows a structurally complex interval. The interval from approximately XX16 to XX38 m has been enlarged and presented in Figure 13 with selected reflectors highlighted to better show the multiple reflector planes

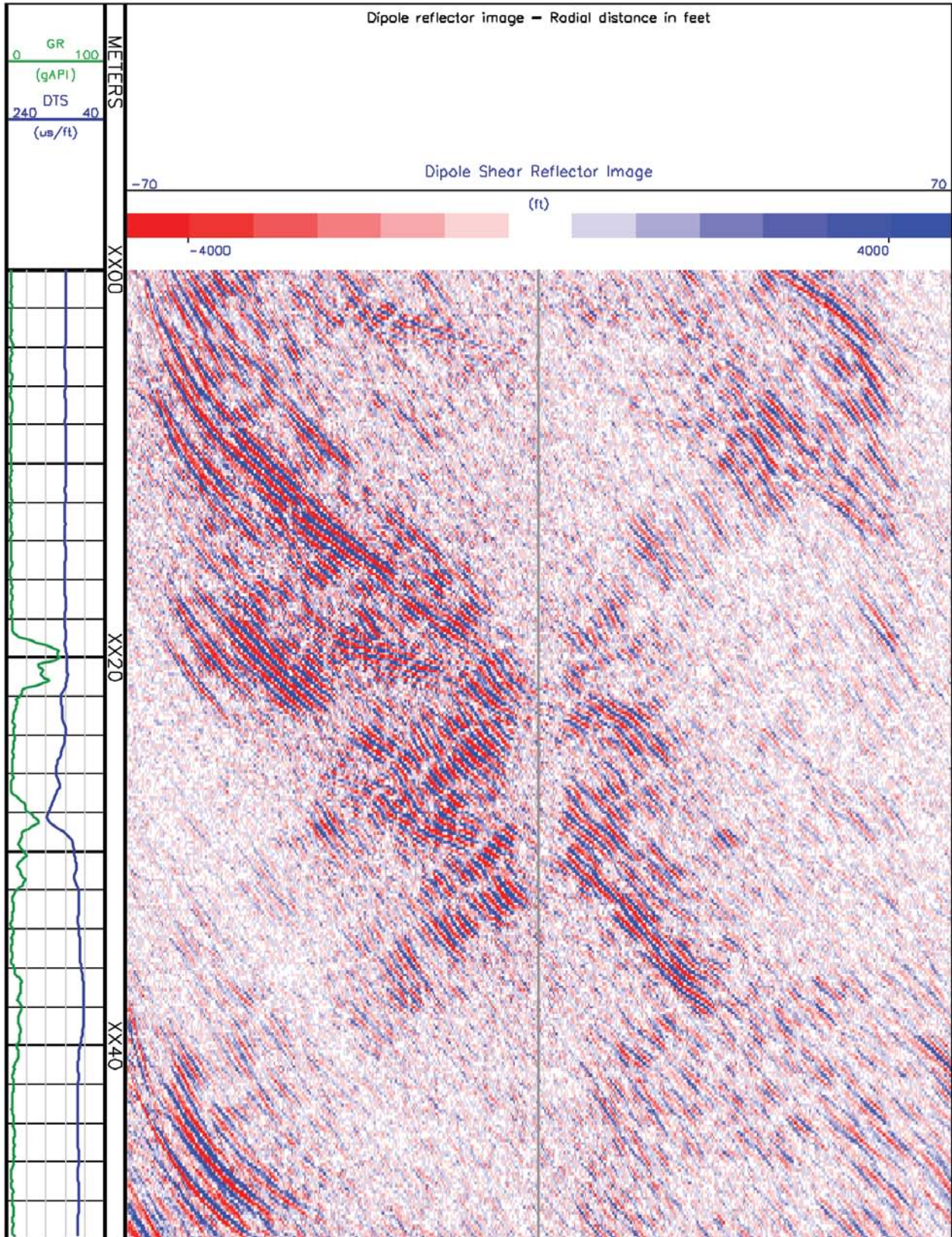


Figure 12 Example of a structurally complex interval where multiple structural planes have been imaged.

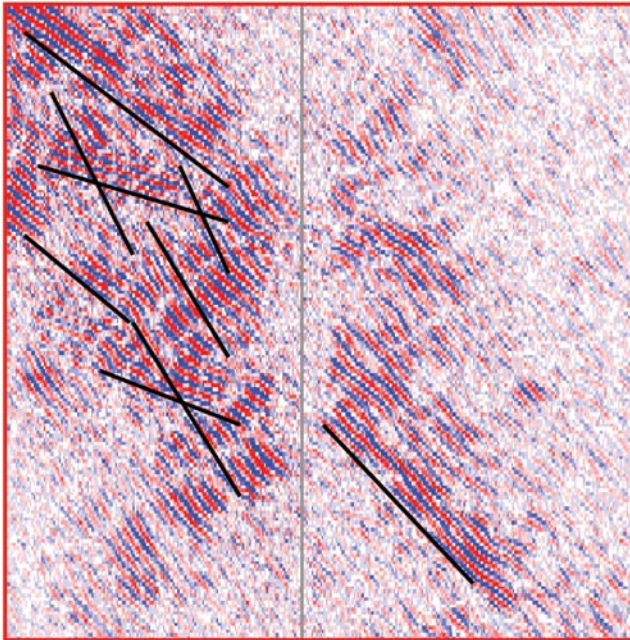


Figure 13 Enlarged section of interval in Figure 12 from XX16-XX38 m with selected structural planes highlighted.

imaged. This demonstrates that structurally complex intervals can be imaged.

Discussion of results

As has been demonstrated the near-wellbore reflection imaging technique using dipole data can be applied to cased holes. However, the technique does have some limitations and signal-to-noise is an important factor in analyzing these faint reflectors. When using inline dipole data it is possible to determine the dip angle of a reflector relative to the borehole but no strike direction can be determined. In a vertical borehole this will be equivalent to the true dip angle of the reflector, however increases in borehole deviation results in some uncertainty in the true dip angle. In a separate investigation from this project, formation dip angles computed from borehole images have been incorporated into other data sets to compare the reflector angles with maximum relative dips and they do show excellent agreement; however this is outside the scope of this article as no image data was recorded over the interval in question.

When cross dipole data is available it can be demonstrated from Eqs. 4a and 4b that the strike angle of the reflector can also be estimated. However, this does still give two possible opposing dip directions. If a borehole image or other dip information is available this will indicate the correct dip direction.

The environment in this case is in many ways ideal for the application of this technique through casing as the formations are relatively homogenous with the reflecting planes having a large difference in acoustic impedance. The

technique has since been applied successfully through casing in some sand/shale sequences. When the technique is applied in openhole the acoustic variation in the formation is much less of a controlling factor.

The technique has many possible applications. As the data used is standard acoustic full-waveform data no additional logging is necessary and therefore this can be performed in addition to any standard acoustic analysis. Here the objective was to identify gas migration paths in an evaporite body, it has also been demonstrated that structural information on a scale between borehole images and borehole seismic has been obtained. From this structural information fracture connectivity can be investigated and structures that do not intersect the wellbore identified. In highly deviated and horizontal wells the technique has been used to determine the proximity of the wellbore to bed boundaries. A future development of the technique will be interactive picking of structural features directly on the computed images.

Conclusions

The above examples demonstrate that it has been possible to image geological structures in a cased borehole by using dipole array acoustic waveform data. Structures up to 70 ft (21.4 m) from the borehole axis have been imaged. In particular, many of the higher-angle structures have been correlated to the gas shows observed in the surface logging data. By using this technique it is possible to generate a fracture connectivity model and hence show migration pathways for the gas within the salt body. This technique also gives structural information on a scale between borehole images and borehole seismic.

Acknowledgements

The author would like to thank Wintershall Noordzee and partners for allowing release of the data presented and for help and advice with preparation of this article. In addition we would like to acknowledge Douglas Patterson from the Baker Hughes Houston Technology Centre and Xiaoming Tang of China University of Petroleum for their assistance with writing of this article and use of many of the figures reproduced in the article.

References

- Hornby, B. 1989, Imaging of near-borehole structure using full waveform sonic data. *Geophysics*, 54(6).
- Meredith, J. [1990] *Numerical and analytical modeling of downhole seismic sources: The near and far field*. PhD dissertation, Massachusetts Institute of Technology.
- Tang, X.M. and Patterson, D. [2009] Single-well S-wave imaging using multi-component dipole acoustic log data. *Geophysics*, 74(6).
- Tang, X.M., Zheng, Y. and Patterson, D. 2007, Processing array acoustic-logging data to image near-borehole geologic structures. *Geophysics*, 72(2), E87-E97.